Stac3 enhances expression of human $Ca_V1.1$ in *Xenopus* oocytes and reveals gating pore currents in HypoPP mutant channels

Fenfen Wu, Marbella Quinonez, Marino DiFranco, and Stephen C. Cannon

Department of Physiology, David Geffen School of Medicine, University of California, Los Angeles, Los Angeles, CA

Mutations of $Ca_V1.1$, the pore-forming subunit of the L-type Ca^{2+} channel in skeletal muscle, are an established cause of hypokalemic periodic paralysis (HypoPP). However, functional assessment of HypoPP mutant channels has been hampered by difficulties in achieving sufficient plasma membrane expression in cells that are not of muscle origin. In this study, we show that coexpression of Stac3 dramatically increases the expression of human $Ca_V1.1$ (plus α_2-δ_{1b} and β_{1a} subunits) at the plasma membrane of *Xenopus laevis* oocytes. In voltage-clamp studies with the cut-open oocyte clamp, we observe ionic currents on the order of 1 µA and gating charge displacements of ∼0.5–1 nC. Importantly, this high expression level is sufficient to ascertain whether HypoPP mutant channels are leaky because of missense mutations at arginine residues in S4 segments of the voltage sensor domains. We show that R528H and R528G in S4 of domain II both support gating pore currents, but unlike other R/H HypoPP mutations, R528H does not conduct protons. Stac3-enhanced membrane expression of $Ca_V1.1$ in oocytes increases the throughput for functional studies of disease-associated mutations and is a new platform for investigating the voltage-dependent properties of $Ca_V1.1$ without the complexity of the transverse tubule network in skeletal muscle.

Journal of General Physiology

INTRODUCTION

Hypokalemic periodic paralysis (HypoPP) is a dominantly inherited disorder of skeletal muscle that presents with recurrent episodes of weakness, typically in association with low serum K^+ (<3.5 mM; Cannon, 2015). During an attack, affected muscle fibers are depolarized and have reduced excitability caused by sodium channel inactivation. The molecular basis of HypoPP is genetically heterogeneous, with ∼60% of families having a missense mutation of *CACNA1S* encoding the α_{1S} subunit of the L-type Ca^{2+} channel, $Ca_V1.1$, whereas another 20% have missense mutations of *SCN4A* encoding the α subunit of the $Na_V1.4$ sodium channel (Sternberg et al., 2001; Miller et al., 2004). Remarkably, all 10 HypoPP mutations of $Na_V1.4$ and 8 of 9 HypoPP mutations in $Ca_V1.1$ are missense substitutions at arginines in S4 transmembrane segments within the voltage sensor domains (Matthews et al., 2009). This convergence strongly supports the prevailing view that recurrent episodes of depolarization-induced weakness in HypoPP are caused by an aberrant inward current conducted by a gating pore leak in the voltage sensor domain of mutant $Ca_V1.1$ or $Na_V1.4$ channels (Cannon, 2010).

A gating pore current was described first in Shaker K^+ channels, where histidine-scanning mutagenesis studies to test for voltage-dependent shifts of proton accessibility to arginine residues in S4 surprisingly created a proton conduction pathway distinct from the K^+-selective pore (Starace and Bezanilla, 2001). Other substitutions of the outermost arginine (R1) in Shaker S4 by amino acids with smaller side groups produced a nonselective cation conductance that was activated by hyperpolarization and permeable to Cs^+, K^+, Li^+, and even guanidinium (Tombola et al., 2005). Conceptually, the anomalous ion conduction pathway is created by misalignment of the S4 R/X mutation and the narrow hydrophobic constriction of the charge transfer center through which the S4 helix translocates during voltage-dependent gating (Moreau et al., 2014). In the case of R1 mutations, the anomalous permeation pathway occurs at hyperpolarized potentials when R1 lies in the hydrophobic waist, and depolarization produces outward movement of S4 that shuts the leak.

Gating pore currents have subsequently been observed for R/X mutations of S4 in Na_V and Ca_V channels, including those associated with HypoPP (Sokolov et al., 2007; Struyk and Cannon, 2007; Jurkat-Rott et al., 2009; Wu et al., 2012). Detecting gating pore currents is more challenging in Na_V and Ca_V channels because each mutant channel has only a single gating pore conductance, unlike the fourfold R/X mutation for homotetrameric Shaker K^+ channels. Gating pore currents conducted by HypoPP mutant channels were initially detected for mutations at R1 and R2 of S4 in domain II for $Na_V1.4$ channels expressed at very high levels in *Xenopus laevis* oocytes (Sokolov et al., 2007; Struyk and Cannon, 2007). The unitary gating pore conductance is

Correspondence to Stephen C. Cannon: sccannon@mednet.ucla.edu

The Rockefeller University Press
J. Gen. Physiol. 2018 Vol. 150 No. 3 475–489
https://doi.org/10.1085/jgp.201711962

estimated to be ∼1,000× smaller than the conductance for Na^+ in the conventional pore formed by the P loop (Mi et al., 2014). Stated another way, gating pore currents recorded under the most favorable conditions at strongly hyperpolarized potentials are only ∼1% of the amplitude of the maximal I_{Na} transient recorded at −10 mV (Sokolov et al., 2007). Anomalous gating pore currents have been reported for all eight $Na_V1.4$ HypoPP mutations studied to date by expression in oocytes, and they have also been detected in voltage-clamped muscle fibers dissociated from $Na_V1.4$-R669H knockin mutant mice (Wu et al., 2011).

Screening $Ca_V1.1$ HypoPP mutant channels for the presence of an anomalous gating pore current has been even more technically demanding. A major obstacle has been that $Ca_V1.1$ does not express well and traffic to the plasma membrane in heterologous systems, which are outside the normal skeletal muscle environment. Moreover, even if HypoPP muscle fibers expressing a $Ca_V1.1$ mutant channel are available, the detection of a gating pore current is compromised by the inability to completely block other endogenous conductances. Limited three-electrode voltage-clamp studies in cut fibers biopsied from patients revealed a 30% increase in the slope conductance at a V_m less than −90 mV for $Ca_V1.1$ HypoPP fibers compared with controls (in a 1-mM K^+, tetrodotoxin (TTX), and Cl^--free bath), consistent with a gating pore current (Jurkat-Rott et al., 2009). We created a $Ca_V1.1$-R528H knockin mutant mouse that has a robust HypoPP phenotype. Under two-electrode voltage clamp of short intact mouse fibers, an increased inward current (∼20%) was observed in $Ca_V1.1$-R528H fibers compared with WT, again consistent with a gating pore leak (Wu et al., 2012). Even with the advantage of a readily available source of HypoPP fibers and the application of a cocktail of blockers to suppress endogenous currents (TTX, TEA, 4-AP, Co^{2+}, Ba^{2+}, and 9-AC), however, the resolution was not sufficient to address important questions such as whether the anomalous inward current was carried by protons or Na^+. More recently, transient expression of human $Ca_V1.1$ ($hCa_V1.1$) in mouse muscle in vivo by local electroporation has revealed a gating pore current primarily carried by protons for $Ca_V1.1$-R1239H (Fuster et al., 2017a), whereas the atypical HypoPP mutation at $Ca_V1.1$-V876E produced a Na^+ leakage current (Fuster et al., 2017b). Again, the total current was increased by only ∼30% in fibers expressing $Ca_V1.1$-V876E, and because of the intrinsic variance for the baseline current density, averaged responses from 50 fibers were used to demonstrate a difference from WT.

A recent development has opened the opportunity for expression and functional characterization of $Ca_V1.1$ in nonmuscle cells. Stac3 (SH3 and cysteine-rich domain 3), a skeletal muscle–specific protein that localizes to the triad, has been shown to be required for excitation–contraction coupling and promotes the expression of $Ca_V1.1$ at the membrane (Horstick et al., 2013; Nelson et al., 2013; Polster et al., 2016). In tsA201 cells that normally do not support the expression of $Ca_V1.1$ at levels sufficient to detect Ca^{2+} currents, coexpression of Stac3 enhances trafficking of $Ca_V1.1$ to the surface membrane and results in a Ca^{2+} current density comparable to that of myotubes (Polster et al., 2015). In the present study, we found that coexpression of Stac3 with $hCa_V1.1$ plus the α_2-δ_{1b} and β_{1a} subunits in *X. laevis* oocytes increased the ionic current several hundredfold, with the gating charge displacement often reaching 1 nC in the cut-open oocyte clamp. This robust level of expression was sufficient to detect gating pore currents in HypoPP mutant $hCa_V1.1$ channels. For two HypoPP-associated mutations in the R1 position of S4 in domain II (R528H and R528G), we show that both give rise to gating pore currents, but permeation of monovalents and a block by divalent cations differ between the two. Unlike other R/H HypoPP mutations in the R1 or R2 position of $Ca_V1.1$ or $Na_V1.4$, the gating pore current in $hCa_V1.1$-R528H channels is not carried primarily by protons.

MATERIALS AND METHODS

Expression of $hCa_V1.1$ channels in oocytes

The human α_{1S} subunit of the skeletal muscle Ca^{2+} channel $hCa_V1.1$ was coexpressed with mouse Stac3, rat α_2-δ_{1b}, and rabbit β_{1a} in *X. laevis* oocytes. The $hCa_V1.1$ cDNA was obtained from the Harvard PlasmID database (accession no. HsCD00347164), Stac3 was a gift from E. Olson (The University of Texas Southwestern Medical Center, Dallas, TX), and the α_2-δ_{1b} and β_{1a} cDNAs were provided by K. Campbell (University of Iowa, Iowa City, IA). The $Ca_V1.1$, β_{1a}, and Stac3 constructs were created in an oocyte-optimized expression vector, pGEMHE (Liman et al., 1992), and the α_2-δ_{1b} construct was made in pcDNA3. Site-directed mutagenesis of $hCa_V1.1$ was performed using the QuikChange II Mutagenesis kit (Agilent) to produce the R528H and R528G HypoPP mutations and the D296K nonconducting background and verified by sequencing the entire cDNA insert and flanking regions of pGEMHE. Approximately 2 ng/nl cRNA was synthesized by in vitro transcription using the mMESSAGE mMACHINE kit (Ambion). Oocytes were harvested by partial oophorectomy and defolliculated in collagenase type I at room temperature for ∼2 h. For coexpression studies, equal volumes of each component cRNA were added into a mixture, and then 50 nl was injected into each oocyte. Injected oocytes were kept at 18°C in 0.5× Leibovitz's L-15 medium (HyClone) supplemented with 1% horse serum, 100 U/ml penicillin, 100 µg/ml streptomycin, and 100 µg/ml amikacin. All experiments were performed within the guidelines established by the University of California, Los Angeles, Institutional Animal Care and Use Committee.

Electrophysiology

Currents were recorded 3–6 d after RNA injection using a cut-open oocyte voltage clamp with the CA-1B amplifier (Dagan) in headstage clamp mode. First, the oocyte was injected with 100 nl of 80 mM BAPTA.K4 plus 10 mM HEPES, pH 7.0, to buffer intracellular Ca^{2+} and thereby suppress endogenous Ca^{2+}-activated Cl^- channels. The oocyte was then mounted in the recording chamber, and the bottom compartment was permeabilized using a brief exposure to 0.1% saponin. The voltage-sensing electrode was positioned just under the dome of the oocyte that protruded into the upper chamber and was filled with a solution containing 3 M sodium methanesulfonate, 10 mM NaCl, and 10 mM HEPES, pH 7.0. The upper and middle guard chambers were actively clamped, and the salt-bridge connections were Cl^- free (1 M sodium methanesulfonate and 10 mM HEPES, pH 7.0). The linear membrane capacitance was compensated by the amplifier's analogue circuitry, but no compensation for the linear leakage current was applied. Current signals were low-pass filtered at 10 KHz for gating-charge displacement measurements and at 1 KHz for ionic current measurements; both were sampled with 16-bit resolution at 20 KHz.

In addition to the injection of BAPTA, all recordings were made in Cl^--free conditions to minimize contributions from endogenous conductances in the oocyte. The internal solution (lower chamber) contained 96 mM KOH and 10 mM HEPES adjusted to pH 7.0 with methanesulfonic acid. The standard external solution, used in both the upper chamber and guard chamber, contained 96 mM NaOH, 6 mM calcium acetate, 10 mM HEPES, and 0.1 mM ouabain titrated to pH 7.0 by methanesulfonic acid. For the ionic current measurements through the $hCa_V1.1$ pore (Figs. 1 and 2), the Ca^{2+} was replaced by 10 mM barium acetate. Gating charge displacement currents were measured by adding 4 mM Co^{2+} to the external solution to block ionic currents through the pore. For the studies on permeability of the gating pore conductance (see Figs. 7 and 8), the external Na^+ was replaced by 110 mM NMDG. For the imposed pH gradients (see Fig. 7), the standard intracellular solution (96 mM potassium methanesulfonate) was acidified to pH 5.0 by replacing HEPES with 10 mM Mes buffer and then adjusting the pH with KOH. The extracellular pH was reduced to 6.5 using methanesulfonic acid, with the HEPES replaced by 20 mM Mes buffer.

Data analysis

The steady-state I-V relation for the Ba^{2+} current conducted by the pore of $hCa_V1.1$ was fit to an ohmic conductance that was scaled by an exponential dependence on channel activation:

$$I_{Ba} = G_{max}(V - E_{rev}) / \left[1 + e^{-(V - V_{1/2})/k}\right],$$

where G_{max} is the maximal conductance, E_{rev} is the reversal potential, $V_{1/2}$ is the half-activation voltage, and k is the steepness factor. Using these parameter values, the relative conductance was computed from the steady-state current as

$$G/G_{max} = I_{Ba}/(V - E_{rev}).$$

The "on" gating charge, Q_{on}, was calculated as the area under the gating charge displacement current elicited by a step change from a holding voltage of −100 mV. The $Q_{on} - V$ relation was fit to a Boltzmann distribution:

$$Q_{on} = Q_{max} / \left[1 + e^{-(V - V_{1/2})/k}\right],$$

where Q_{max} is the maximal Q_{on}, $V_{1/2}$ is the voltage at which half the total charge has moved, and k is the steepness factor.

In all figures, error bars represent ±SEM. The confidence for an observed difference between two means was assessed with a two-tailed t test; for tests of three means, the ANOVA with Bonferroni correction was used.

RESULTS

Ionic currents were measured in a cut-open oocyte voltage clamp in the absence of added Ca^{2+} with 10 mM external Ba^{2+} as the divalent charge carrier. In Fig. 1, leak subtraction of linearly scaled responses to a 20-mV depolarization from the holding potential of −100 mV was used to suppress background leakage currents and residual linear capacitance transients. For control oocytes in which the $hCa_V1.1$ cRNA was omitted but all other subunit transcripts (β_{1a}, α_2-δ_{1b}, and Stac3) were coinjected, only miniscule inward currents were observed with a fast transient amplitude of ∼5 nA (Fig. 1 A). When Stac3 was omitted but the Ca^{2+} channel transcripts ($hCa_V1.1 = \alpha_{1S}$, β_{1a}, and α_2-δ_{1b}) were coinjected, current amplitudes were still only ∼10 nA, but then had the slow kinetics and voltage dependence expected for L-type Ca^{2+} channels (Fig. 1 B). Enormous currents with amplitudes that were ∼100× larger were observed for oocytes coinjected with cRNA for Stac3 plus WT Ca^{2+} channel transcripts (Fig. 1, C and D). The brief positive transient current at 1 ms in Fig. 1 D is the nonlinear charge displacement of the voltage sensors in $hCa_V1.1$. The Ba^{2+} current density was on the order of 25 A/F for WT $hCa_V1.1$ based on the linear capacitance for the dome of the oocyte under a voltage clamp of 56 ± 4.0 nF. The inward current transients for WT channels did not inactivate during the 250-ms depolarization (or even during longer pulses up to several seconds; Fig. S1), whereas in the absence of Stac3, inactivation was readily observed (Fig. 1 B, inset). Stac3 has been reported to also inhibit inactivation of $Ca_V1.2$ expressed in tsA201 cells (Polster et al., 2015). Expression of two HypoPP mutant channels with missense mu-

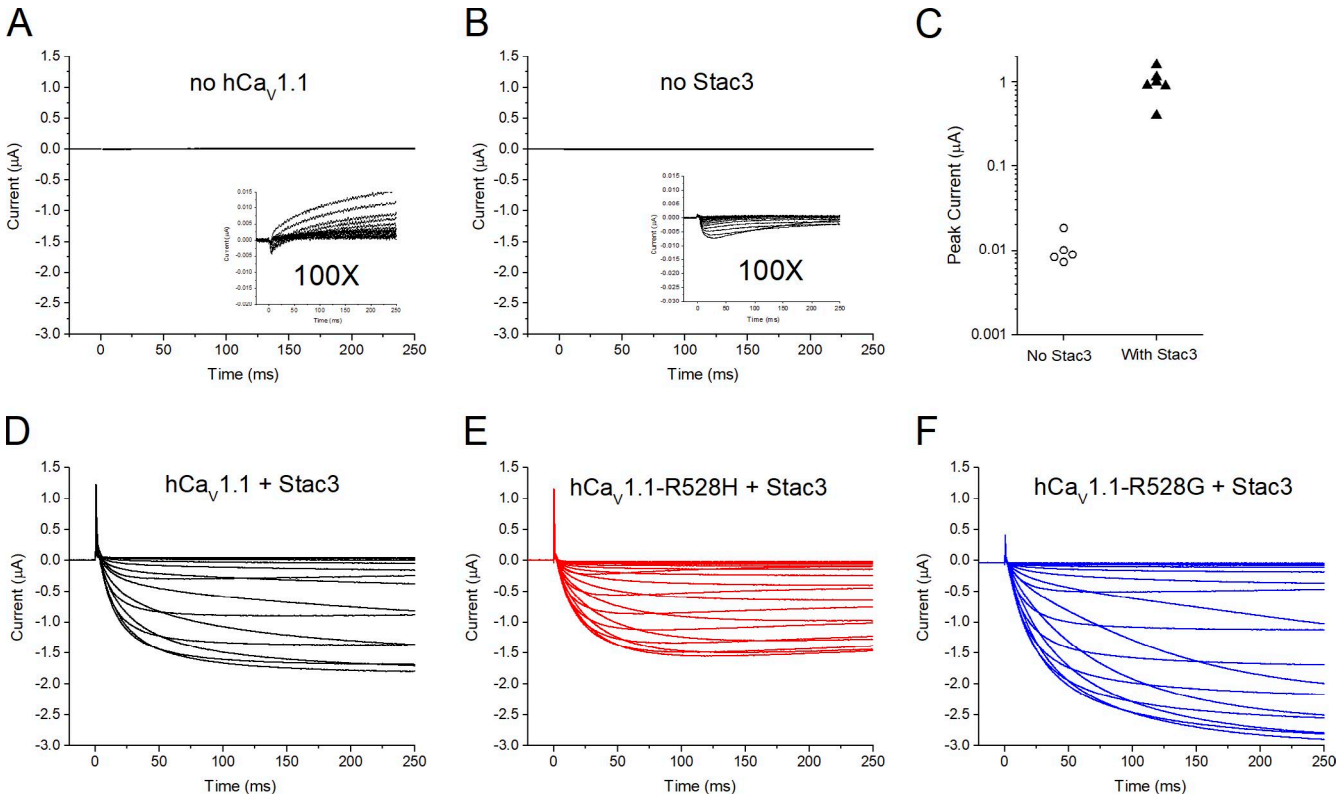

Figure 1. **Coexpression of Stac3 dramatically enhances hCa$_V$1.1 currents in *X. laevis* oocytes.** Each panel shows currents recorded in a cut-open oocyte clamp with 10 mM Ba^{2+} as the divalent charge carrier. Step depolarizations to −50 mV through 40 mV were applied from a holding potential of −100 mV. Linear leak correction was performed by scaling and subtracting the response to a 20-mV depolarization. **(A)** Currents from an oocyte injected with RNA for Stac3, α_2-δ_{1b}, and β_{1a} subunits; inset shows the same traces at 100×. **(B)** Currents recorded when α_{1S} (hCa$_V$1.1), α_2-δ_{1b}, and β_{1a} subunits were expressed, but no Stac3. At high gain (100×), slow Ca^{2+} channel currents were detectable in the absence of Stac3. **(C)** Maximal inward current observed from oocytes injected with Ca^{2+} channel subunits with Stac3 (closed triangles) or without Stac3 (open circles). Each symbol represents a separate oocyte, and all were recorded from the same batch. **(D–F)** Large robust currents were consistently observed in oocytes coexpressing Stac3 with hCa$_V$1.1 (WT or HypoPP mutants), α_2-δ_1, and β_{1ab} subunits.

tations at hCa$_V$1.1-R528 in S4 of domain II also resulted in robust ionic currents (Fig. 1, E and F), with peak amplitudes that tended to be smaller for R528H (−1.20 ± 0.091 μA) and larger for R528G (−1.9 ± 0.25 μA) compared with WT (−1.62 ± 0.17 μA), although these values were not statistically different at the 0.05 level (ANOVA).

The ionic current conducted by the hCa$_V$1.1 subunit was isolated pharmacologically to determine the voltage dependence of channel activation. Fig. 2 shows a block of currents recorded in 10 mM Ba^{2+} by application of 10 μM nifedipine (Fig. 2 A) or 4 mM Co^{2+}(Fig. 2 B). The residual current was small in the presence of blockers, demonstrating that the majority of the measured ionic current was conducted by hCa$_V$1.1, and the residual current was consistently smaller in the presence of Co^{2+} compared with nifedipine. For the concentrations used, we interpret this difference to represent a more complete block by Co^{2+} than nifedipine; therefore, in other protocols designed to detect gating pore currents or to measure gating charge displacement currents, we used Co^{2+} as the pore blocker.

The voltage dependence for activation of the Ca^{2+} channel constructs was measured as the Co^{2+}-sensitive current elicited by a 250-ms depolarization (range of −50 to 40 mV) from a holding potential of −100 mV (Fig. 2 C). The maximal inward current occurred at a test potential that was left shifted (more negative) for both R528H (V_{test} = 15 mV) and R528G (10 mV) compared with WT hCa$_V$1.1 (25 mV). The steady-state I-V response for each oocyte was fit by a Boltzmann-scaled linear conductance to estimate the $V_{1/2}$, steepness factor k, maximal conductance G_{max}, and reversal potential E_{rev}, as summarized in Table 1. The midpoint for activation was left shifted by ∼15 mV for HypoPP mutants (R528H, 2.5 ± 2.2 mV, $P < 0.001$; R528G, −2.6 ± 0.55 mV, $P < 0.001$) compared with WT (16 ± 1.3 mV). The maximal conductance, G_{max}, was smaller for R528H mutant channels (32 ± 2.1 μS, $P < 0.001$) compared with WT (78 ± 9.2 μS), as reflected by the smaller slope in Fig. 2 C for voltages >25 mV. Although the maximal inward current was more negative for R528G channels than WT (Fig. 2 C), it was not because of a larger G_{max}

for the mutant channel (Table 1). The larger currents for R528G channels were a consequence of the left shift for activation, which caused these channels to open at more negative potentials where there was a larger driving force for Ba^{2+} influx. Note that the limiting slope conductance at depolarized potentials was comparable for R528G and WT channels. The relative conductance plot, G/G_{max} in Fig. 2 D, removes the effect of the driving force and more clearly shows the left shift for activation of mutant channels.

Table 1. **Voltage dependence of channel activation**

$Ca_V1.1$ construct	$V_{1/2}$	k	G_{max}	E_{rev}
	mV	*mV*	*μS*	*mV*
WT	16 ± 1.3	6.8 ± 0.34	78 ± 9.2	52 ± 2.0
R528H	2.5 ± 2.2	7.1 ± 0.31	32 ± 2.1	58 ± 2.6
R528G	−2.6 ± 0.55	6.0 ± 0.16	61 ± 5.6	46 ± 1.5

The high expression level for $hCa_V1.1$ at the oocyte plasma membrane provided an opportunity to mea-

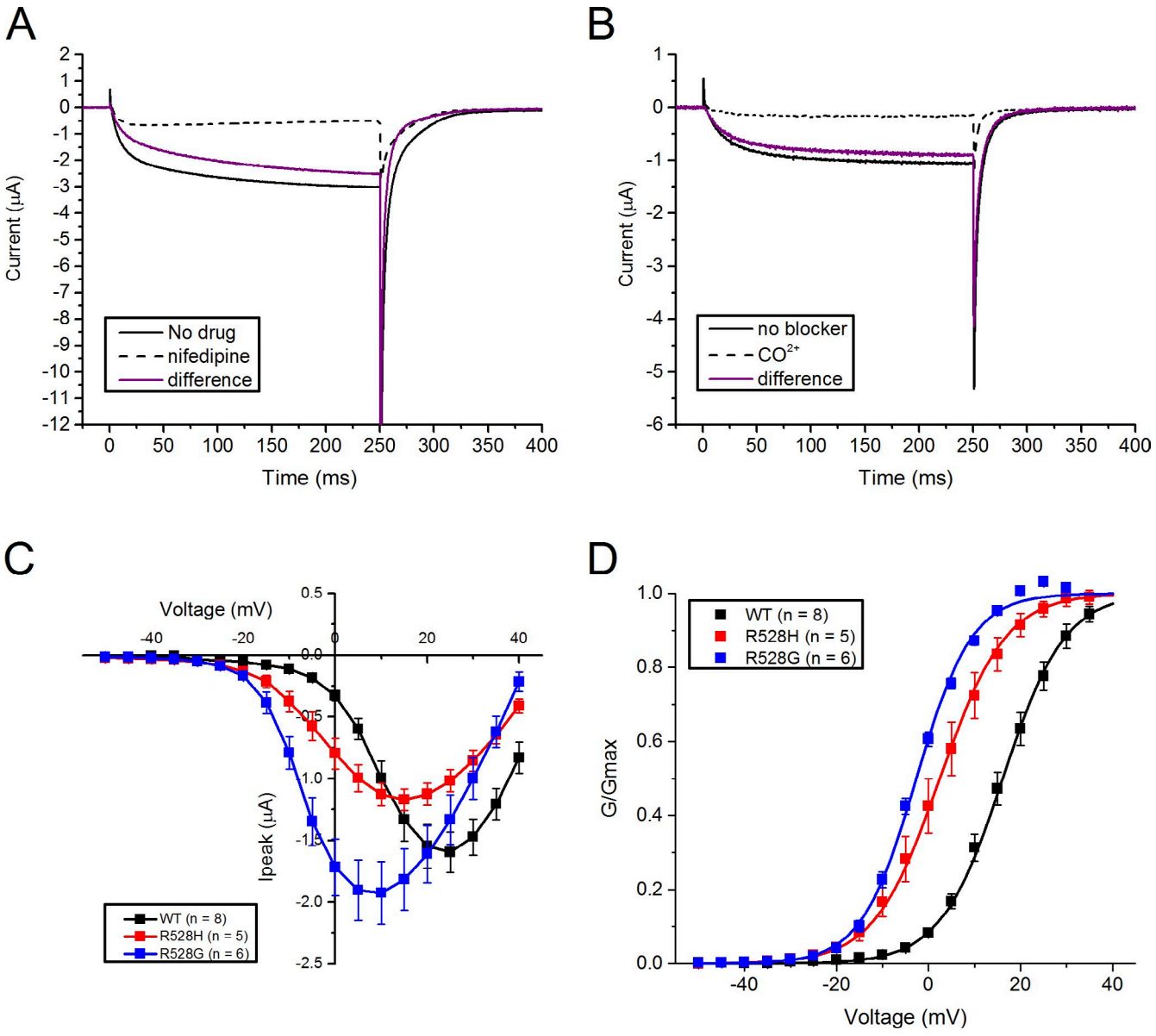

Figure 2. **Activation of $hCa_V1.1$ currents is hyperpolarized for HypoPP channels. (A and B)** The majority of the current recorded from oocytes expressing Stac3, $hCa_V1.1$ α_2-δ_{1b}, and β_{1a} subunits was conducted by $hCa_V1.1$, as shown by a block with 10 μM nifedipine (A) or with 4 mM Co^{2+} (B). Traces show leak-subtracted currents recorded in 10 mM Ba^{2+} for depolarization to 20 mV from a holding potential of −100 mV. **(C)** Steady-state I-V relation for Co^{2+}-sensitive current with 10 mM Ba^{2+} as the charge carrier. Currents were elicited by depolarization from a holding potential of −100 mV. Symbols are mean values, and smooth lines show the Boltzmann fit using the mean values of the parameters. Error bars represent ±SEM. **(D)** The hyperpolarized shift of activation for HypoPP mutant channels is shown more clearly by plotting relative conductance, $G/G_{max} = I/[G_{max} \cdot (V - E_{rev})]$, as a function of test potential.

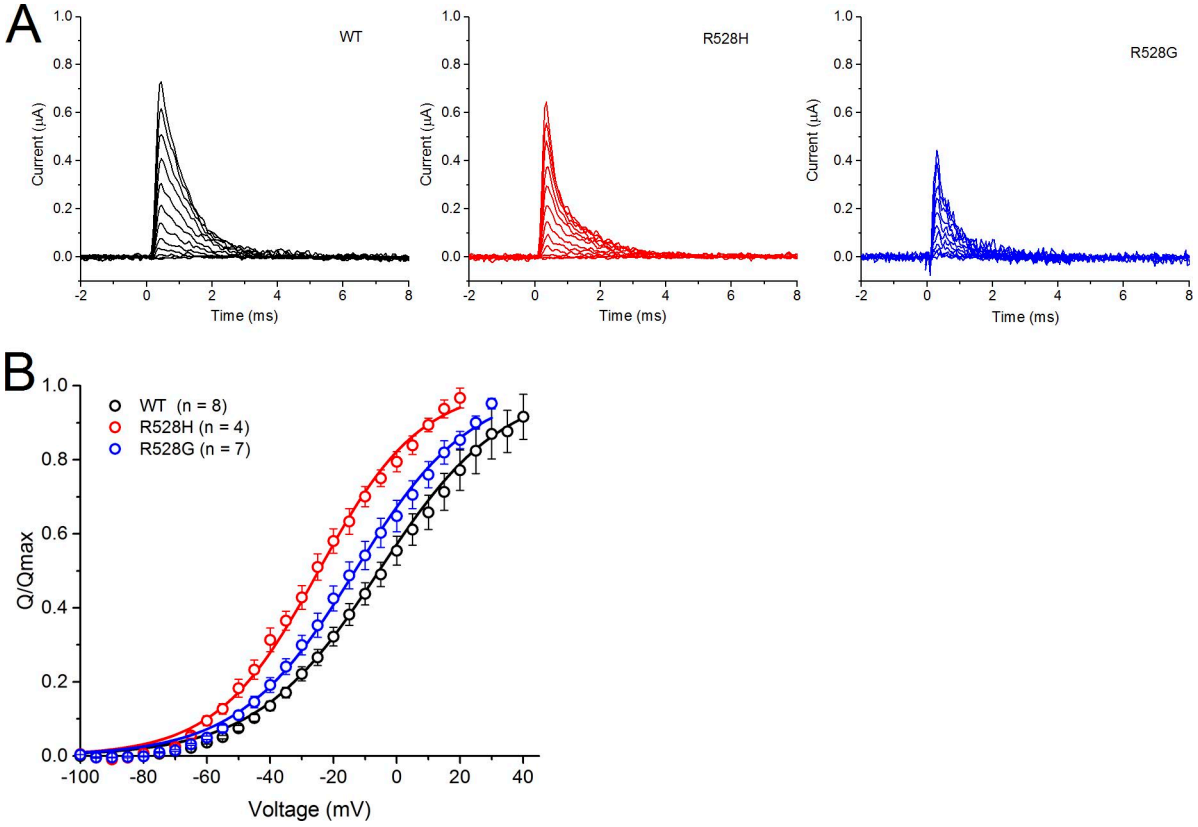

Figure 3. **Gating charge displacement had a left-shifted voltage dependence for HypoPP mutant channels. (A)** Gating charge displacement currents were recorded in 2 mM Co^{2+} to block ionic currents. Traces show the superposition of leak-subtracted responses for step depolarizations of −100 to 20 mV in 10-mV increments from a holding potential of −100 mV. **(B)** The "on" gating charge, calculated from the area under the charge displacement currents in A, was normalized to the maximum and plotted as a function of test potential. Smooth curves show Boltzmann functions using mean values for the parameters of the fit to each oocyte, and error bars represent ±SEM. The midpoint of activation for Q/Q_{max} was left shifted by 19 mV for R528H and by 7.4 mV for R528G compared with WT.

sure the gating charge displacement current without the usual complications (i.e., poor voltage clamp for the transverse tubular membrane and contributions from other voltage-gated ion channels in skeletal muscle fibers). Ionic current through the $hCa_V1.1$ pore was blocked with Co^{2+}, and charge displacement currents were measured as the residual after scaling and subtracting the linear capacitance currents elicited by a 20-mV depolarization from a holding potential of −100 mV (Fig. 3 A). These "on" gating charge displacement currents typically had a maximal peak amplitude of 500–800 nA and often exceeded 1 μA. The charge displacement, obtained by integrating the current transient, was saturated for large depolarizations. On average, the maximal charge displacement, Q_{max}, for WT channels (0.69 ± 0.06 nC) was larger than that of HypoPP mutant channels (R528H, 0.25 ± 0.10 nC, $P < 0.005$; R528G, 0.36 ± 0.07 nC, $P < 0.005$). The voltage dependence of the charge displacement was left shifted by nearly 20 mV for R528H (−25 ± 2.3 mV, $P < 0.0005$) compared with WT (−5.6 ± 1.5 mV), and a smaller shift was detected for R528G (−13 ± 3.4 mV, $P < 0.05$), as shown in Fig. 3 B.

Our initial strategy to determine whether the HypoPP mutant channels conduct gating pore currents was to measure the time-averaged current in the interval of 3–4 ms after the onset of a test pulse, without online leak subtraction. This approach was designed to select a time interval wherein the gating charge displacement was essentially complete; hence, a voltage-dependent transition for gating pore access would also be complete, and yet, the sluggish opening of the conventional pore (α current) would still be lagging. $Ca_V1.1$ pore blockers were not used because it is not possible to predict a priori whether these compounds might also block an anomalous gating pore conductance. Fig. 4 A (middle and right) shows exemplary current traces and demonstrates the larger holding current of HypoPP mutant channels at −100 mV with a correspondingly larger spread of steady-state current amplitudes in response to voltage steps from −120 to 10 mV. At the most depolarized potentials in this series, the inward Ba^{2+} current conducted by the $hCa_V1.1$ pore was readily apparent (Fig. 4 A, green traces). The I-V relation for the time-averaged current over the interval of 3–4 ms (Fig. 4 A,

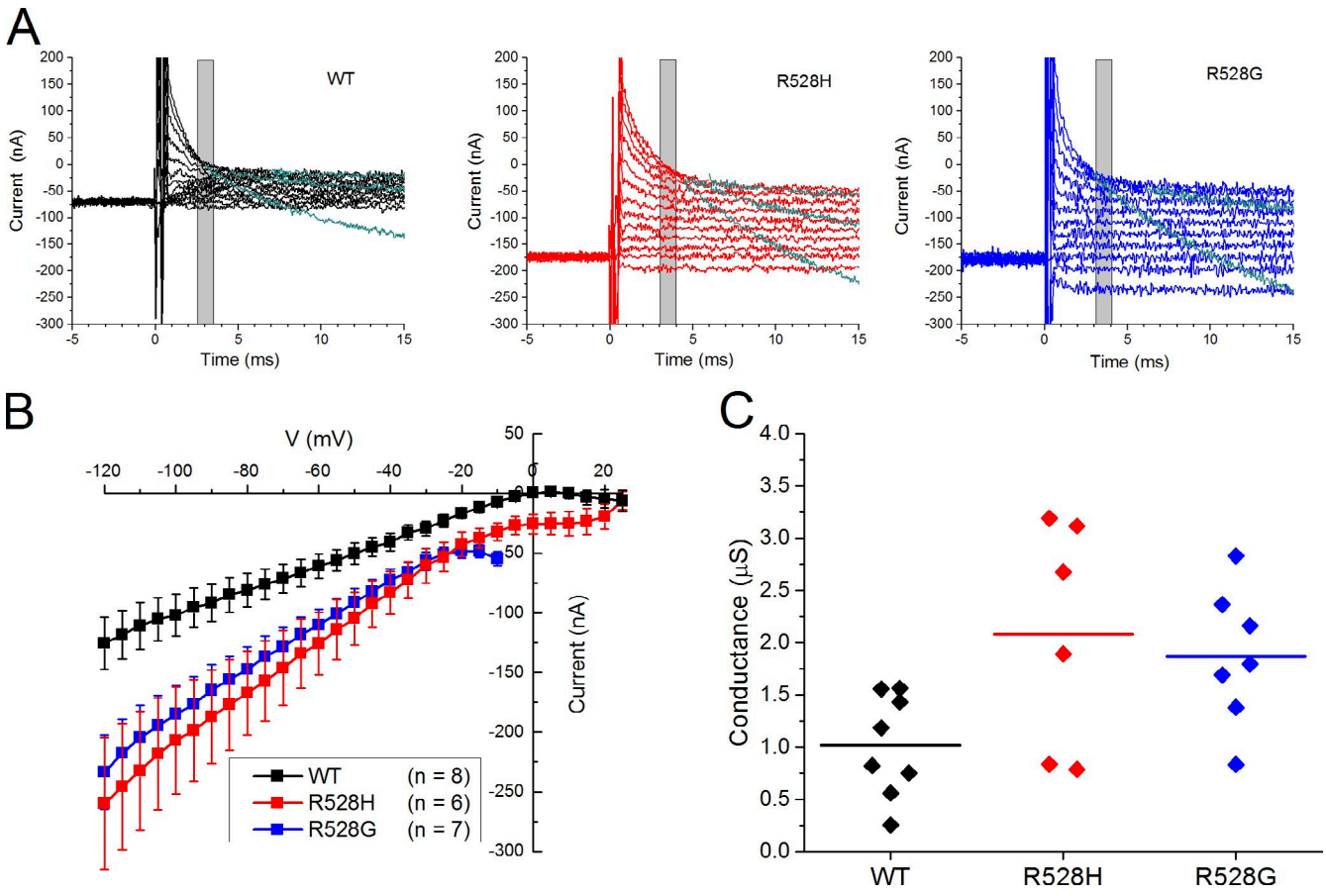

Figure 4. **Larger inward currents, consistent with an anomalous gating pore conductance, were observed for R528H and R528G HypoPP mutant channels. (A)** Exemplary traces shown for currents recorded in response to test potentials of −120 to 20 mV in 10-mV increments from a holding potential of −100 mV. At the more depolarized test potentials, the onset of Ba^{2+} current conducted by the conventional pore of $Ca_V1.1$ channels was detected (green traces). No leak subtraction was performed. **(B)** Isochronal current, measured in the interval of 3–4 ms after the onset of the test pulse (shaded bars in A), is plotted as a function of test potential. Inward currents at hyperpolarized potentials were larger for R528H and R528G than WT. Error bars represent ±SEM. **(C)** The slope conductance, based on a linear fit of the I-V relation on the interval of −120 to −20 mV, was larger for oocytes expressing R528H and R528G than for WT. Symbols show responses for individual oocytes, and horizontal lines show the mean values.

shaded bar) was approximately linear from −120 to −20 mV (Fig. 4 B), with a larger slope conductance for HypoPP mutant channels than WT (R528H, 2.1 ± 0.44 μS, $P < 0.05$; R528G, 1.9 ± 0.25 μS, $P < 0.05$; WT, 1.0 ± 0.15 μS). Over this voltage range, the conventional pore of $Ca_V1.1$ is essentially closed, and so our interpretation is that the nonspecific background leakage current of the cut-open oocyte is ∼1 μS (Fig. 4 B, WT). The recordings for WT $hCa_V1.1$ were from the same batches of oocytes used to express HypoPP mutant channels, with mutant and WT trials interdigitated, and so we believe the background nonspecific currents were comparable. We propose that the approximately twofold higher conductance for oocytes expressing the HypoPP $hCa_V1.1$ subunits is caused by the additional contribution from an anomalous gating pore conductance that is open at hyperpolarized potentials.

In terms of signal detection, the magnitude of the gating pore conductance is approximately equal to that of the nonspecific component, and so the ability to detect a twofold change in current amplitude is required to observe the consequence of a HypoPP mutation. Fig. 4 C shows the variability in our conductance measurements, in which the response of each oocyte is presented as a separate point. The higher mean values for the HypoPP mutants compared with that of WT were statistically different (ANOVA with Bonferroni correction, $P < 0.05$).

The I-V relation in Fig. 4 B gives the appearance of inward rectification, as would be expected for a gating pore conductance caused by a mutation in the R1 or R2 position of S4 that is permissive for ion flow at hyperpolarized potentials and closes with depolarization. In our experimental conditions, however, this effect is more likely to be caused by activation of the conventional pore, with Ba^{2+} influx producing a flattening of the I-V relation. This interpretation is consistent with the flattening effect also being present for WT chan-

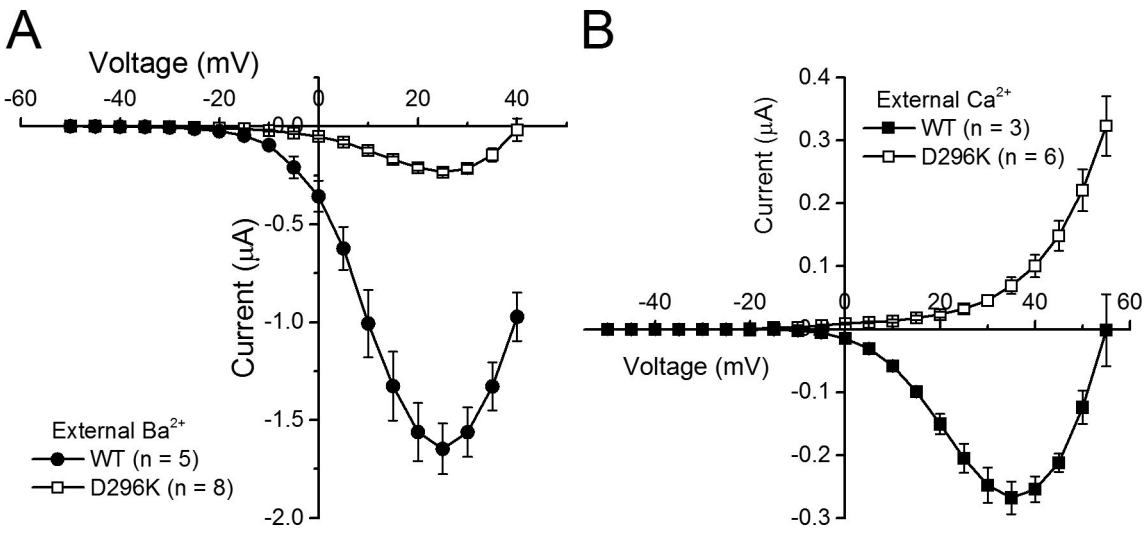

Figure 5. **The D296K hCa$_V$1.1 subunit conducts Ba^{2+} poorly and is nonconducting in Ca^{2+}. (A)** Steady-state current amplitude recorded in 10 mM external Ba^{2+} (no added Ca^{2+}) for a series of 250-ms test depolarizations from a holding potential of −100 mV. Current amplitude is greatly reduced for D296K compared with WT channels, but the voltage dependence of activation is similar. **(B)** In 10 mM external Ca^{2+} (no Ba^{2+}), no inward current was detected for D296K channels. Subtraction of a linearly scaled leak response to a depolarization from −100 to −80 mV was used to remove the nonspecific leakage current. Error bars represent ±SEM.

nels, which do not support a gating pore conductance, and also with the need to truncate the R528G curve at −10 mV because at more depolarized potentials, an obvious Ba^{2+} current was observed for this mutation with the greatest left shift of activation (Fig. 2).

Nonconducting variants of Ca$_V$1.1 have been identified in zebrafish (Schredelseker et al., 2010), and we introduced the D296K substitution into the hCa$_V$1.1 subunit because a background construct that lacks Ca^{2+} influx through the conventional pore would be well suited for the detection of gating pore currents. Residue D296 is highly conserved in Ca$_V$ channels and is the fourth residue downstream from the consensus E in domain I for the EEEE selectivity filter. Membrane expression levels were comparable for WT and D296K channels based on Q_{max} values of 0.75 ± 0.08 nC for WT (n = 4) and 0.75 ± 0.07 nC for D296K (n = 6). In 10 mM Ba^{2+} (no added Ca^{2+}), a residual inward current was observed for D296K channels (Fig. 5 A), with the amplitude being 13% of that for WT channels (D296K, −0.23 ± 0.017 μA; WT, −1.6 ± 0.13 μA; $P < 0.001$). We suspected that the nonconducting state might require block by binding of Ca^{2+} in the external vestibule of D296K channels. Indeed, there was no detectable inward current in 10 mM Ca^{2+} for oocytes expressing D296K channels, whereas oocytes expressing WT channels had a maximal inward current of 0.27 μA at a test potential of 35 mV (Fig. 5 B). We used this nonconducting D296K construct in the presence of external Ca^{2+} as the background channel from which to ascertain the presence of anomalous inward currents for HypoPP mutant channels (DK/R528H or DK/R528G) as compared with the hCa$_V$1.1 channels that did not contain a HypoPP mutation (DK/WT).

Divalent cations are low-affinity, voltage-dependent blockers of gating pore currents conducted by Na$_V$1.4 HypoPP mutant channels (Sokolov et al., 2010; Francis et al., 2011). Similarly, we noticed that the holding current at −100 mV was reduced when Co^{2+} was added to block Ca^{2+} currents in hCa$_V$1.1-R528H channels. A more complete investigation of the Co^{2+} block is shown for DK HypoPP and WT channels in Fig. 6. The raw current traces without leak subtraction (Fig. 6 A) show that in DK/R528H channels, no inward Ca^{2+} currents were detected, even for membrane depolarization to 20 mV for 25 ms. In contrast, without the DK background, inward currents were apparent within 5 ms of a depolarization to −10 mV (Fig. 4 A, middle). Addition of 2 mM Co^{2+} produced an obvious decrease in the holding current for oocytes expressing DK/R528H channels at −100 mV and attenuated the steady-state current elicited at all test potentials from −120 to 20 mV (Fig. 6 A, right). No attenuation of the current by Co^{2+}, however, was observed for DK/WT or DK/R528G channels. The steady-state I-V relation for representative oocytes that were in 6 mM Ca^{2+}, and then switched to 4 mM Ca^{2+} plus 2 mM Co^{2+}, is shown in Fig. 6 B. As expected for a gating pore leak, oocytes expressing DK/R528H or DK/R528G had larger currents compared with DK/WT. The block of the DK/R528H current by 2 mM Co^{2+} was comparable at all test potentials, unlike the strongly voltage-dependent divalent block of rat Na$_V$1.4-R666G (R2 in domain II), which occurred only at voltages less than −80 mV (Sokolov et al., 2010). On average, the slope conductance (−100 to −40 mV) for DK/R528H decreased from 5.7 ± 0.57 μS (n = 9) in 6 mM Ca^{2+} to 3.9 ± 0.47 μS in 4 mM Ca^{2+} plus 2 mM Co^{2+}, whereas the

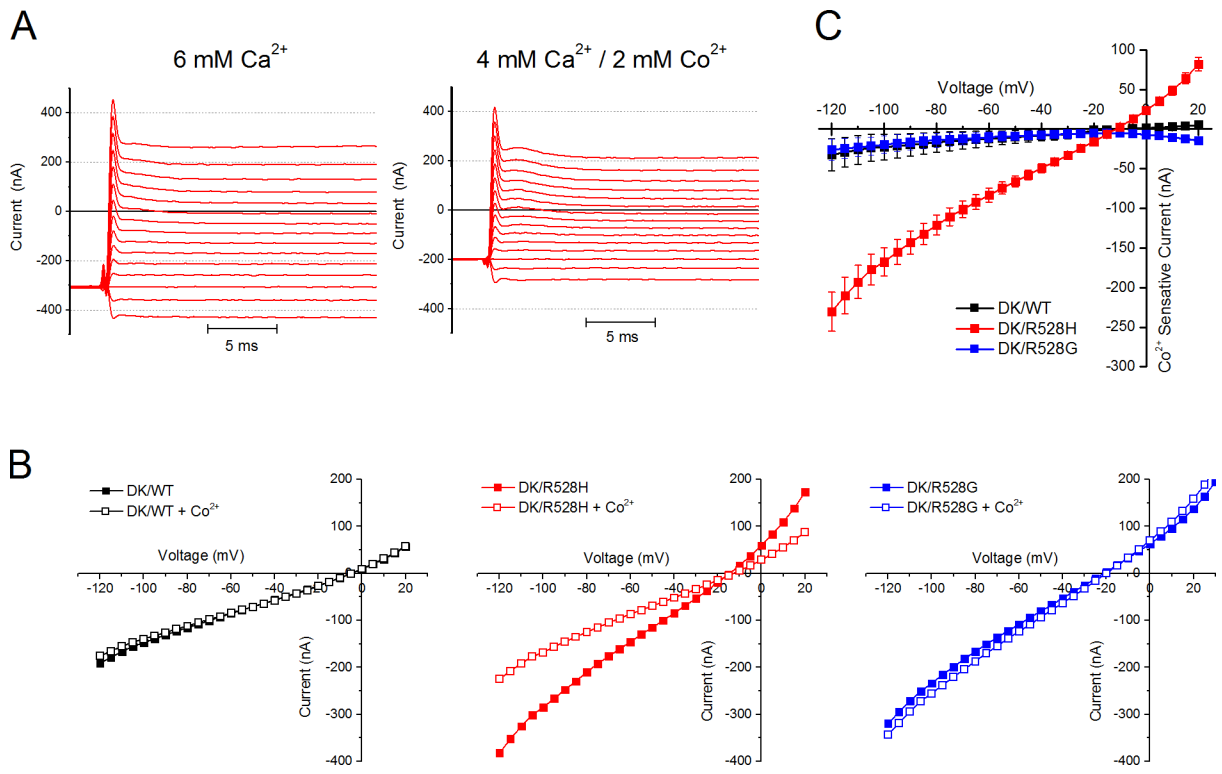

Figure 6. **Block of DK/R528H gating pore current by Co^{2+}. (A)** Currents recorded from an oocyte expressing DK/R528H channels in Ca^{2+} (left) or Ca^{2+} plus Co^{2+} (right). The oocyte was held at −100 mV, and currents elicited by test pulses from −120 to 20 mV are shown. Capacitance was partially cancelled by the amplifier, but no analogue or digital leak subtraction was performed. **(B)** Representative steady-state I-V relation for individual oocytes expressing DK/WT, DK/R528H, or DK/R528G. Closed symbols show control response in 6 mM Ca^{2+}; open symbols show control response after bath exchange to 4 mM Ca^{2+} and 2 mM Co^{2+}. **(C)** The Co^{2+}-sensitive current was calculated from the difference of responses in 6 mM Ca^{2+} minus those in 4 mM Ca^{2+} plus 2 mM Co^{2+}. Symbols show mean with SEM error bars for *n* = 9 DK/WT-, 9 DK/R528H-, and 6 DK/R528G-expressing oocytes.

conductance for DK/WT channels in 6 mM Ca^{2+} was 2.4 ± 0.36 µS (n = 9). If it is assumed that the nonspecific component (i.e., not from a gating pore) of the total conductance in DK/R528H channels equals the total conductance observed in DK/WT oocytes, then 2 mM Co^{2+} caused a 55% block of the DK/R528H gating pore current: 100% × [1 − (3.9 − 2.4 µS)/(5.7 − 2.4 µS)]. Trials with addition of 2 mM Ni^{2+} did not reveal a significant block (<2%) of the gating pore current for the histidine-containing mutation R528H (Fig. S2). The I-V relation for the gating pore current, as defined by the subtraction of background currents in WT-expressing oocytes from the same batch, was indistinguishable for recordings with 6 mM Ca^{2+} or 10 mM Ba^{2+} as the external divalent (Fig. S3). This observation implies that the gating pore current for DK/R528H and DK/R528G channels is not blocked by Ba^{2+}.

The Co^{2+}-sensitive currents obtained by subtraction from control responses in 6 mM Ca^{2+} are shown in Fig. 6 C. This separation of currents by a block likely represents the optimal available method for isolating the current passed by an anomalous conduction pathway in R528H mutant channels, presumably the gating pore leak, from the other background currents in the oocyte. Unexpectedly, the Co^{2+}-sensitive current was linear over the entire voltage range, up to the maximum potential of 20 mV. Gating pore currents in Shaker K^+ channels and $Na_V1.4$, however, show inward rectification because the anomalous conductance is occluded when depolarization translocates the mutant residues in S4 (R1 or R2) out of the hydrophobic gating charge transfer center. One possible explanation for the lack of detectable rectification in our measurements is that S4 of domain II in $Ca_V1.1$ moves outward at more positive potentials. Unfortunately, for voltages >20 mV, an outward rectifying current occurs in DK channels (Fig. 5 B), which confounds the measurement. This outward current appears to be a K^+ efflux from the oocyte, as the external Ca^{2+} block in mutant DK channels is relieved by depolarization.

Substitutions of arginines in S4 by histidine often results in a proton-selective gating pore current. The HypoPP mutations R669H and R672H in domain II of $Na_V1.4$ (R1 and R2) both create a proton-selective gating pore conductance (Struyk and Cannon, 2007; Struyk et al., 2008), and the R1239H HypoPP mutation in domain IV of $hCa_V1.1$ (R1) is permissive for proton influx (Fuster et al., 2017a). We tested whether the

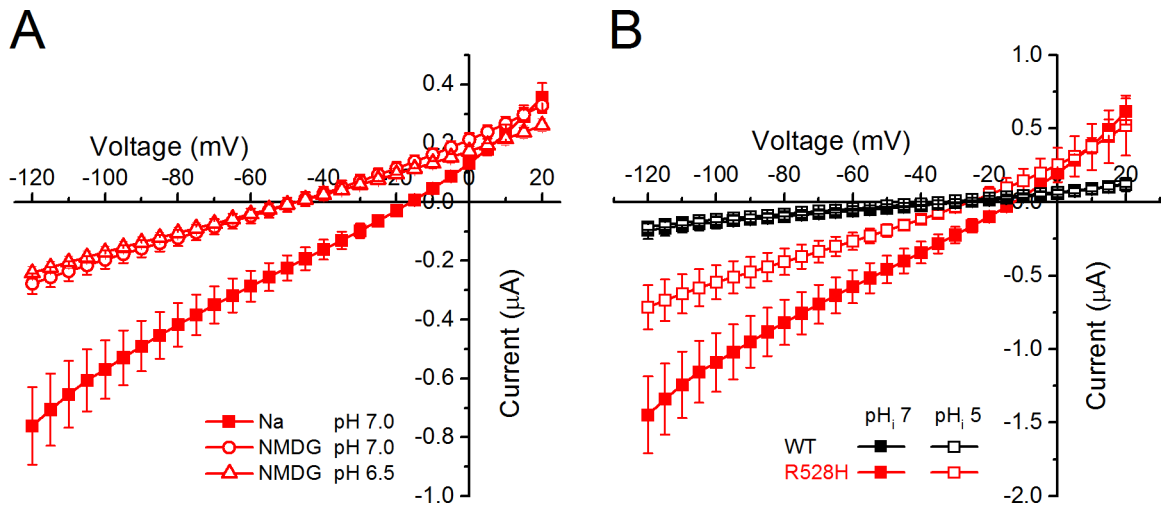

Figure 7. **The gating pore current in DK/R528H channels is carried primarily by Na^+. (A)** Steady-state currents elicited by 20 ms–step depolarizations from a holding potential of −100 mV in oocytes expressing DK/R528H channels. Currents were initially recorded in external 96 mM Na^+ (closed squares). The bath was exchanged with a 110-mM NMDG solution, and then currents were recorded again (open circles). Finally, the external pH was decreased to 6.5, and the pulse protocol was repeated a third time (open triangles). Symbols show means with SEM error bars; n = 5 oocytes. **(B)** Steady-state current recorded in external Na^+ with a symmetrical pH gradient of 7.0 (closed squares), and then repeated after the lower chamber bathing the permeabilized segment of the oocyte was replaced by Mes-buffered solution with pH 5.0. Symbols show mean for DK/WT- (black, n = 3) and DK/R528H- (red, n = 6) expressing oocytes.

anomalous inward current for $Ca_V1.1$-R528H was carried by protons by measuring the change in current for DK/R528H channels in response to substitution of the extracellular cation or by shifting the pH gradient across the oocyte (Fig. 7). The steady-state I-V relation for DK/R528H-expressing oocytes was measured in the same egg for three different external ionic conditions. First, currents were measured in 96 mM external Na^+ at pH 7.0; next, the bath was exchanged with a 110-mM NMDG solution at pH 7.0; and finally, the external pH was decreased to 6.5 while still in NMDG. Replacement of external Na^+ by NMDG caused a large reduction of inward current and shifted the reversal potential by −31 ± 6 mV (Fig. 7 A). The slope conductance (−100 to −40 mV) decreased from 6.7 ± 1.1 μS in Na^+ to 3.7 ± 0.27 μS in NMDG. These changes show that much of the inward current was carried by Na^+. In contrast, the inward current was identical when Na^+ was replaced by NMDG for the proton-selective gating pore currents conducted by the $Na_V1.4$ R/H HypoPP mutations in domain II (Fig. 8 in Struyk et al., 2008). Moreover, in DK/R528H-expressing oocytes, increasing the external [H^+] threefold while in NMDG did not increase the inward current or cause a shift in the reversal potential (Fig. 7 A, open triangles). In another set of oocytes, we increased intracellular protons by replacing the HEPES-buffered solution at pH 7.0 in the lower chamber (where the oocyte was permeabilized with saponin) with a Mes-buffered bath at pH 5.0. Currents recorded from DK/R528H-expressing oocytes in 96 mM external Na^+ were decreased by 46 ± 7% (n = 6) with intracellular acidification (Fig. 7 B), whereas DK/WT currents were not affected. Only a modest −8.9 ± 2.9–mV shift in the reversal potential occurred for DK/R528H oocytes, whereas if the full intracellular decrease of 2 pH units had been achieved, the calculated shift in the reversal potential for H^+ would have been −116 mV. The internal pH of the permeabilized oocyte is unlikely to have attained the full change of 2.0 units, and direct measurement with a pH-sensing microelectrode is necessary when precise knowledge of the pH gradient is critical (Starace and Bezanilla, 2001). We previously showed, however, that a proton-selective gating pore current becomes outward (positive) using this same technique in $Na_V1.4$ HypoPP mutant channels (Struyk and Cannon, 2007). Thus, intracellular acidification predominantly causes a partial block of the gating pore current rather than shifting the reversal potential. Collectively, we interpret the effects of Na^+/NMDG exchange and of shifts in the proton gradient on DK/R528H currents as evidence that the anomalous inward current is carried primarily by Na^+ with a negligible contribution from protons.

The gating pore leak created by some R/X mutations in S4 is permeable to the guanidinium ion, perhaps because of the loss of a native guanidinium group in the mutated arginine residue. In fact, for the HypoPP mutations R672G and R672H at the R2 position of $Na_V1.4$, guanidinium has a higher permeability than Na^+ or K^+ (Sokolov et al., 2010). We tested whether guanidinium is also permeable for the HypoPP mutations at R528 of $hCa_V1.1$. Currents were initially recorded in NMDG and again recorded after the external bath was replaced by a

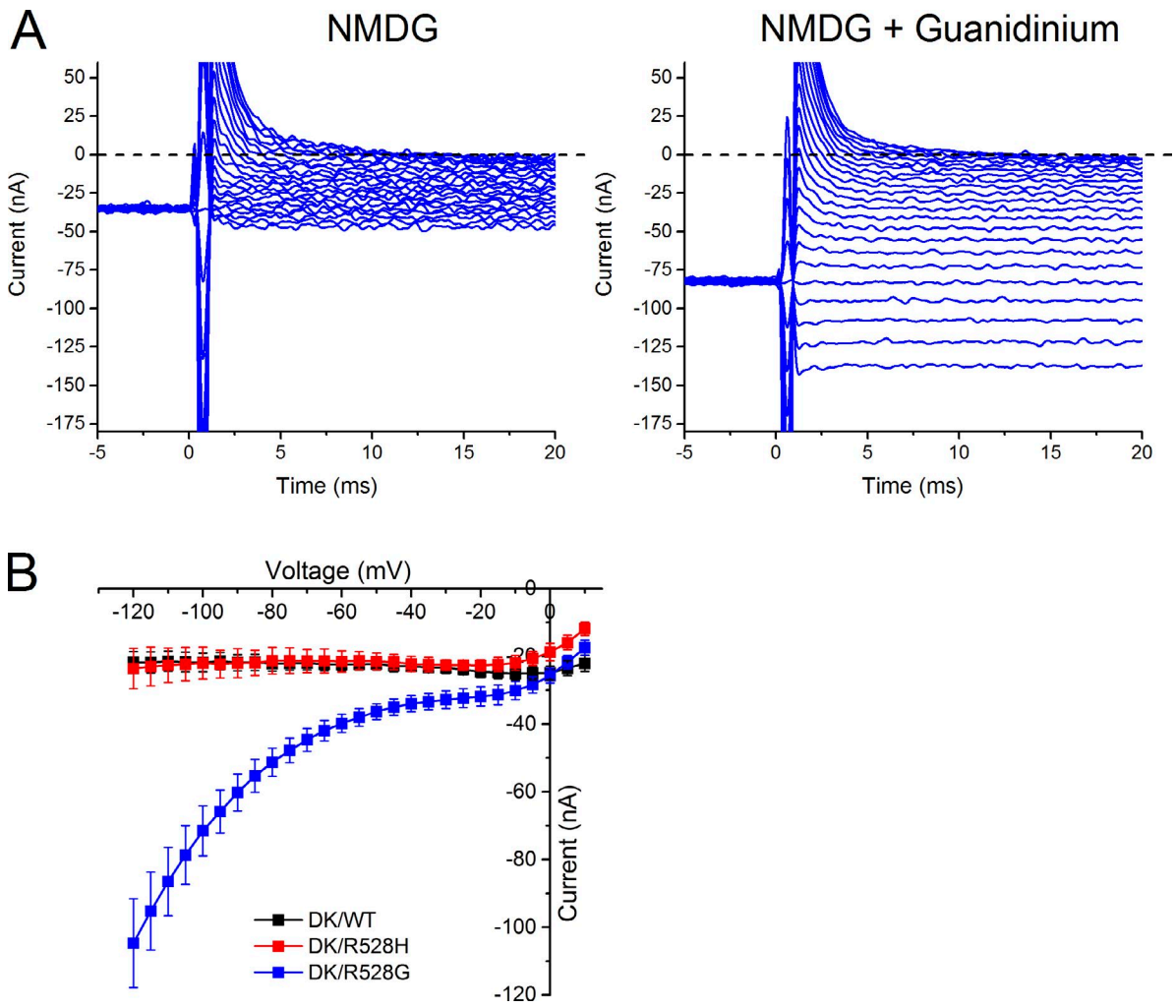

Figure 8. **The DK/R528G gating pore is permeable to guanidinium. (A)** Currents were recorded from DK/R528G channels in 110 mM NMDG and then in 60 mM NMDG plus 60 mM guanidinium. Traces show responses elicited by step depolarizations of −120 to 10 mV in 5-mV increments from a holding potential of −100 mV. No leak subtraction was used. **(B)** The steady-state current recorded in NMDG was subtracted from the current in guanidinium plus NMDG and plotted as a function of test potential. Symbols show mean values for oocytes expressing DK/WT (n = 5), DK/R528H (n = 4), or DK/R528G (n = 5) channels. Error bars represent ±SEM.

1:1 mixture of NMDG and guanidinium. For DK/R528G channels, currents increased with the addition of guanidinium and showed inward rectification (Fig. 8 A). This guanidinium current was not present in DK/WT or DK/R528H channels, as illustrated by the I-V relation in Fig. 8 B, which shows the steady-state current recorded in guanidinium minus that from NMDG alone.

DISCUSSION

The primary objective of this study was to determine whether oocyte expression of hCa$_V$1.1 at the plasma membrane could be enhanced sufficiently by coexpression of Stac3 so that gating pore currents in channels with R/X mutations of S4 could be unambiguously detected in the cut-open voltage clamp. The advantages of such a system are that (a) screening of untested Ca$_V$1.1 HypoPP mutations can be greatly accelerated and less burdensome than existing systems in mouse muscle, and (b) in contrast to muscle, the *X. laevis* oocyte has a much quieter electrical environment with fewer voltage-gated endogenous conductances and lacks the complexity of the transverse tubules. Prior voltage-clamp studies of Na$_V$1.4 HypoPP mutant channels in the cut-open oocyte revealed gating pore currents that scaled linearly with channel expression level. The gating pore current density (amplitude/Q_{max}) was 50–100 nA/nC at −140 mV (Struyk and Cannon, 2007; Struyk et al., 2008). Therefore, we anticipated that the expression level of hCa$_V$1.1 would require a Q_{max} of at least 0.2 nC, corresponding to a predicted gating pore current of 10–20 nA superimposed on the typical nonspecific leakage current of ∼100 nA at −100 mV. In practice, with an expression level of Q_{max} = ∼0.3 nC, we observed

an increased inward current of ~100 nA for HypoPP compared with WT $hCa_V1.1$ (Fig. 4 B).

The biggest challenge for reliably detecting a gating pore current is distinguishing this anomalous current from the nonspecific leakage current inherent to any voltage-clamp experiment. Our first approach was to simply compare the I-V relation for oocytes expressing HypoPP and WT $hCa_V1.1$ without using the linear leak or offset subtraction. Care was taken to use the same batch of oocytes and alternate recordings from HypoPP, and WT-expressing eggs were made on the same day. The assumption is that, with this approach, the nonspecific leak will be identical, and any deviation in the I-V from WT can be attributed to the HypoPP mutations. Differences in expression level of WT versus HypoPP channels could have potentially confounded the comparison. First, based on the Q_{max}, the expression of channels with WT $hCa_V1.1$ was about twofold greater than that for either R528H or R528G, and yet, the inward currents were larger for these HypoPP mutant constructs. The second line of evidence for an anomalous current in R528H-expressing oocytes was block by either external Co^{2+} (Fig. 6 B) or internal protons (Fig. 7 B) that did not occur for WT $hCa_V1.1$. Third, a large inward guanidinium current was conducted by R528G-expressing oocytes (Fig. 8), but not by WT or R528H. Moreover, block by divalent cations and permeability to guanidinium are established features of gating pore currents in $Na_V1.4$ (Sokolov et al., 2010) and Shaker K^+ channels (Tombola et al., 2005). Collectively, these observations support our interpretation that the increased inward currents detected at hyperpolarized potentials with Stac3-enhanced expression of $hCa_V1.1$-R528H and $hCa_V1.1$-R528G, compared with WT $hCa_V1.1$, are anomalous gating pore currents. The amplitude of the gating pore currents was comparable for $hCa_V1.1$-R528H and $hCa_V1.1$-R528G (Figs. 4 and 6 B), which is consistent with the clinical observation that HypoPP attack frequency, duration, and severity are comparable for patients with R528H (Miller et al., 2004) and R528G (Wang et al., 2005).

Measurement of gating pore currents from HypoPP $hCa_V1.1$ mutant channels expressed in oocytes improves the resolution and the ability to characterize the permeation properties compared with studies in muscle fibers. These improvements are primarily a consequence of the greatly reduced repertoire of endogenous voltage-gated conductances in oocytes compared with muscle. For example, the amplitude of gating pore currents in mouse fibers transfected with $hCa_V1.1$-R1239H was ~35% greater than the residual background current in low Cl^-, TEA, TTX, and 4-AP (Fuster et al., 2017a) and only ~20% greater in our homozygous knockin $Ca_V1.1$-R528H mutant mouse (Wu et al., 2012). Population averages from 10 to 40 fibers were used to detect a difference in currents from HypoPP versus WT fibers. Conversely, for $hCa_V1.1$ expressed in oocytes, the increased inward current for HypoPP mutant channels was 100% of WT controls (Figs. 4 and 6 B) or even greater (Fig. 7 B). When the HypoPP mutant $hCa_V1.1$ expression level was high (>0.5 nC), the large holding current required to clamp the oocyte at −100 mV revealed a clearly anomalous response from a single measurement.

With oocytes, the larger amplitude of gating pore currents relative to the background leak and the reduced need for channel blockers enabled us to determine permeation properties, which we were not able to discern in two-electrode voltage-clamp recordings from $Ca_V1.1$-R528H mouse fibers. Unexpectedly, the gating pore current in $hCa_V1.1$-R528H was carried primarily by Na^+. A highly proton-selective gating pore conductance is created by HypoPP mutations at R1 and R2 in S4 of domain II in $Na_V1.4$ (Struyk and Cannon, 2007; Struyk et al., 2008), by an arrhythmogenic mutation at R1 in domain I of $Na_V1.5$ (Gosselin-Badaroudine et al., 2012b), and by the R/H substitution at R1 in Shaker (Starace and Bezanilla, 2004). Similarly, the HypoPP mutation $Ca_V1.1$-R1239H at R2 of S4 in domain IV supports a gating pore current mainly carried by protons (Fuster et al., 2017a). Other HypoPP mutations at arginines in S4 of $Na_V1.4$ (i.e., substitutions by residues other than histidine) produce nonselective gating pore conductances that are permeable to monovalent cations (Struyk et al., 2008). In a clinical context, the ionic selectivity of gating pore conductances associated with HypoPP mutations has been a puzzle. First, the clinical manifestations of HypoPP are identical, with no discerning signs or symptoms for those with proton-selective versus monovalent cation–nonselective gating pore leaks (Cannon, 2015). Second, carbonic anhydrase inhibitors such as acetazolamide are often effective at reducing the frequency and severity of attacks; yet, for a subset of mutations, the drug may worsen symptoms (Sternberg et al., 2001; Matthews et al., 2011). However, this variable response to carbonic anhydrase inhibitors does not correlate with proton selectivity of the gating pore current. As efforts to understand genotype–phenotype relations in HypoPP continue, it is important to be aware that the most frequently encountered mutation, $Ca_V1.1$-R528H, does not follow the expected pattern of proton selectivity for R/H mutations in S4. Model simulations support the notion that the depolarized reversal potential of the gating pore current, relative to the normal resting potential of muscle, is the critical feature for causing HypoPP rather than the particular ion that carries the current (Cannon, 2015).

The gating pore conductance created by the mutation of R1 or R2 in S4 to a smaller amino acid residue is often more permeable to guanidinium than to monovalent metal cations (e.g., Cs^+, Na^+, and K^+). For example, R1C in Shaker and R2H/G in domain II of $Na_V1.4$ read-

ily conduct guanidinium. An inwardly rectifying gating pore current, while in a solution of 80 mM TEA plus 38 mM guanidinium, was also reported for the HypoPP mutation $Ca_V1.1$-R528G expressed in GLT cells (Bednarz et al., 2016). In our oocyte expression system, an inwardly rectifying guanidinium current was observed for $hCa_V1.1$-R528G, but not for $hCa_V1.1$-R528H or WT $hCa_V1.1$ (Fig. 8). Thus, the biophysical properties of the gating pore current for $hCa_V1.1$-R528H are distinct from those observed with most other R/H mutations in $Ca_V1.1$, $Na_V1.4$, $Na_V1.5$, or Shaker: (a) Na^+ is the predominant charge carrier, not H^+; (b) the current is not blocked by 2 mM Ni^{2+}; and (c) the gating pore is not permeable to guanidinium.

Gating pore currents usually have a pronounced voltage dependence, with the permissive conformation being at hyperpolarized potentials for mutations at R1 of Shaker (Starace and Bezanilla, 2004; Tombola et al., 2005) and at R1 or R2 of S4 in Na_V channels (Sokolov et al., 2005; Gosselin-Badaroudine et al., 2012a). This inward rectification has not been as well documented for gating pore currents in Ca_V channels. In voltage-clamp studies of $hCa_V1.1$-HypoPP fibers (Ruff, 1999; Jurkat-Rott et al., 2009), the Kir current, which is likely to be the main source of inward rectification in those recordings, was not blocked. Our prior two-electrode voltage-clamp studies of $Ca_V1.1$-R528H knockin mutant mouse fibers had a small inward current that activated around −20 mV (Fig. 6 A in Wu et al., 2012), most likely from a residual contribution by partially blocked $Ca_V1.1$ channels. This current produced a flattening of the I-V relation in the −20- to 20-mV range and thereby contributed to the appearance of inward rectification of the gating pore current. The whole-cell silicone-clamp technique used by Fuster et al. (2017a) to record currents from mouse fibers transiently expressing $hCa_V1.1$-R1239H was more effective at blocking endogenous conductances, but there was almost no discernable rectification to the gating pore current, except when a steep gradient was imposed for the permeant ion.

Similarly, we did not detect inward rectification for gating pore currents recorded in oocytes expressing $hCa_V1.1$-R528H or $hCa_V1.1$-R528G. The flattening of the I-V relation between −20 and 20 mV in Fig. 4 B is primarily caused by the onset of an inward Ba^{2+} current through the conventional pore rather than inward rectification. The apparent rectification was absent from subsequent records in the $hCa_V1.1$ DK nonconducting background (Figs. 6 and 7). Intriguingly, the paradigm with the best separation of the gating pore current from nonspecific background leakage currents, namely the Co^{2+}-sensitive current in DK/R528H channels (Fig. 6 C), has a linear I-V from −100 to 20 mV. This implies that the gating pore current was still active at a membrane potential 45 mV depolarized from the midpoint (−25 mV) of the *Q(V)* relation. Either the gating pore leak created by mutations of R1 in domain II conducts ions in both the resting and activated states of S4, or the motion of S4 from the resting state is impeded by the R1 mutation. The latter seems unlikely because, although Q_{max} was reduced, the conventional pore opened with depolarization and conducted large currents (Fig. 1, E and F). The pronounced inward rectification observed for $hCa_V1.1$-R528G in external guanidinium (Fig. 8) is attributed to the asymmetry of the permeant ion (i.e., no internal guanidinium). We attempted to resolve these issues with a nonconducting $hCa_V1.1$ subunit that would eliminate the Ca^{2+} current and thereby allow us to test for inward rectification of the gating pore current at very depolarized potentials. The D296K construct was partially successful in that no Ca^{2+} current was activated during 20-ms depolarizations of up to 20 mV (Fig. 6 A), compared with the inward current within 5 ms of a depolarization to 0 mV for the WT background (Fig. 4 A). With larger step depolarizations (>20 mV), however, a prominent outward rectifying current was present (Fig. 5 B) that scaled with the expression level of DK channels. We interpret this as voltage-dependent relief of external Ca^{2+} block and efflux of internal K^+ through DK channels. Attempts to dialyze out the internal K^+ were not successful at reducing the outward current. In summary, although we are confident that anomalous gating pore currents are conducted by $hCa_V1.1$ with HypoPP R1H/G mutations in domain II, the question remains open of whether depolarization and outward movement of S4 attenuates this current to produce inward rectification. The depolarization of V_{rest} during a HypoPP attack is caused by the net balance of currents over a voltage range of −90 to −50 mV, and so the presence or absence of rectification for the gating pore current at depolarized potentials is not expected to impact the mechanistic basis for episodic weakness.

The Stac3-enhanced membrane expression of $hCa_V1.1$ in oocytes also provided an opportunity to characterize the ionic current through the conventional pore and gating charge displacement current at high resolution. Moreover, the cut-open oocyte clamp avoids two important complications of recording $Ca_V1.1$ currents from muscle fibers. First, the voltage-clamp control of the cut-open oocyte is much better than for the transverse tubules in muscle (Kim and Vergara, 1998); second, the complication of Ca^{2+} depletion in the transverse tubes (Friedrich et al., 2001) is prevented. Consistent with these advantages, our current traces were more similar to those from myotubes than adult muscle fibers. Specifically, very little or no inactivation of an ionic current was observed (Fig. 1, E and F), presumably in part by avoiding ion depletion in the transverse tubule, and the decay of Q_{on} charge displacements was much faster (Fig. 3).

We used Ba^{2+} as the charge carrier to measure the I-V relation (Figs. 1 and 2), as well as Cl-free solutions,

to attenuate a contribution from Ca^{2+}-activated Cl channels. A reduced G_{max} for HypoPP mutant channels, as observed here (Table 1), is a consistent finding from many different experimental systems. The R528H mutation engineered into the rabbit $Ca_V1.1$ and expressed in Ltk^- cells (Lapie et al., 1996) or oocytes without Stac3 (Morrill and Cannon, 1999) had a 40–60% reduction of G_{max}; however, no reduction was reported for expression in GLT cells (Jurkat-Rott et al., 1998). The results in myotubes cultured from patients showed either slightly reduced G_{max} (Morrill et al., 1998) or no change (Jurkat-Rott et al., 1998), with the caveat that these cells are heterozygous for WT and R528H. In homozygous fibers from our knockin R528H mouse, G_{max} was reduced by 53% (Wu et al., 2012). In general, the reduced G_{max} is paralleled by a reduction in Q_{max}, which implies the defect is with the expression at the membrane rather than with the impaired coupling of charge movement to the channel opening. Fewer data are available for R528G, which is a much rarer HypoPP mutation, but a reduced G_{max} was observed in our study and for rabbit $Ca_V1.1$-R528G expressed in GLT cells (Bednarz et al., 2016). A hyperpolarized shift in the voltage dependence of activation, as detected in our oocyte system (Fig. 2 D), has also been reported in oocytes without Stac3 (Morrill and Cannon, 1999), R528G in GLT cells (Bednarz et al., 2016), and human R528H/WT myotubes (Jurkat-Rott et al., 1998). A hyperpolarized shift in the voltage dependence of charge displacement was also detected (Fig. 3). For R528H, the shift in the *Q(V)* relation can entirely account for the shift of the *G(V)*. With R528G, however, the 7.4-mV hyperpolarized shift in *Q(V)* was considerably smaller than the 18.6-mV shift of *G(V)*, which suggests that the coupling between charge movement and channel opening was affected.

Overall, the functional defects of HypoPP mutant channels observed for our Stac3-enhanced expression system in oocytes are in agreement with results from prior studies of R528H and R528G using human myotubes, knockin mice, or transfected GLT cells. This comparison includes ionic currents conducted through the pore, charge displacement, and gating pore currents. With the advantages of the oocyte expression system, we were able to make the first determination of ion selectivity for HypoPP mutations at R528. The remarkably high expression level of $hCa_V1.1$ in the Stac3/oocyte system, plus the fidelity of preserving channel biophysical behavior, will greatly accelerate the functional testing of other $hCa_V1.1$ mutations associated with HypoPP. In addition, the Stac3/oocyte system is an ideal preparation for studying the modulatory effect of accessory subunits, domain-specific coupling of S4 movement to channel opening, and other biophysical studies of $Ca_V1.1$ channels.

ACKNOWLEDGMENTS

We thank the members of Riccardo Olcese's laboratory for assistance with oocyte preparation and for advice on optimizing the recording of Ca^{2+} currents in the cut-open oocyte clamp.

This work was supported by a grant from the National Institute of Arthritis and Musculoskeletal and Skin Diseases of the National Institutes of Health (AR-063128).

The authors declare no competing financial interests.

Author contributions: The experimental design was conceived by F. Wu, M. DiFranco, and S.C. Cannon. F. Wu performed the cut-open voltage-clamp experiments, and M. Quinonez and F. Wu created the mutant constructs. M. DiFranco optimized the system for recording Ca^{2+} currents. F. Wu, M. Quinonez, M. DiFranco, and S.C. Cannon participated in the analysis and interpretation of the data. S.C. Cannon wrote the paper.

Eduardo Ríos served as editor.

Submitted: 30 November 2017
Accepted: 3 January 2018

REFERENCES

Bednarz, M., Y. Da, F. Lehmann-Horn, C. Fan, J. Schallner, and K. Jurkat-Rott. 2016. Skeletal muscle calcium channel mutation R528G: enhanced channel inactivation and omega-current at hyperpolarization contribute to hypokalemic periodic paralysis. *Neurological Research and Therapy.* 1:20–30. https://doi.org/10.14302/issn.2470-5020.jnrt-16-993

Cannon, S.C. 2010. Voltage-sensor mutations in channelopathies of skeletal muscle. *J. Physiol.* 588:1887–1895. https://doi.org/10.1113/jphysiol.2010.186874

Cannon, S.C. 2015. Channelopathies of skeletal muscle excitability. *Compr. Physiol.* 5:761–790. https://doi.org/10.1002/cphy.c140062

Francis, D.G., V. Rybalchenko, A. Struyk, and S.C. Cannon. 2011. Leaky sodium channels from voltage sensor mutations in periodic paralysis, but not paramyotonia. *Neurology.* 76:1635–1641. https://doi.org/10.1212/WNL.0b013e318219fb57

Friedrich, O., T. Ehmer, D. Uttenweiler, M. Vogel, P.H. Barry, and R.H. Fink. 2001. Numerical analysis of Ca2+ depletion in the transverse tubular system of mammalian muscle. *Biophys. J.* 80:2046–2055. https://doi.org/10.1016/S0006-3495(01)76178-4

Fuster, C., J. Perrot, C. Berthier, V. Jacquemond, and B. Allard. 2017a. Elevated resting H+ current in the R1239H type 1 hypokalaemic periodic paralysis mutated Ca2+ channel. *J. Physiol.* 595:6417–6428. https://doi.org/10.1113/JP274638

Fuster, C., J. Perrot, C. Berthier, V. Jacquemond, P. Charnet, and B. Allard. 2017b. Na leak with gating pore properties in hypokalemic periodic paralysis V876E mutant muscle Ca channel. *J. Gen. Physiol.* 149:1139–1148. https://doi.org/10.1085/jgp.201711834

Gosselin-Badaroudine, P., L. Delemotte, A. Moreau, M.L. Klein, and M. Chahine. 2012a. Gating pore currents and the resting state of Nav1.4 voltage sensor domains. *Proc. Natl. Acad. Sci. USA.* 109:19250–19255. https://doi.org/10.1073/pnas.1217990109

Gosselin-Badaroudine, P., D.I. Keller, H. Huang, V. Pouliot, A. Chatelier, S. Osswald, M. Brink, and M. Chahine. 2012b. A proton leak current through the cardiac sodium channel is linked to mixed arrhythmia and the dilated cardiomyopathy phenotype. *PLoS One.* 7:e38331. https://doi.org/10.1371/journal.pone.0038331

Horstick, E.J., J.W. Linsley, J.J. Dowling, M.A. Hauser, K.K. McDonald, A. Ashley-Koch, L. Saint-Amant, A. Satish, W.W. Cui, W. Zhou, et al. 2013. Stac3 is a component of the excitation-contraction coupling machinery and mutated in Native American myopathy. *Nat. Commun.* 4:1952. https://doi.org/10.1038/ncomms2952

Jurkat-Rott, K., U. Uetz, U. Pika-Hartlaub, J. Powell, B. Fontaine, W. Melzer, and F. Lehmann-Horn. 1998. Calcium currents and transients of native and heterologously expressed mutant skeletal muscle DHP receptor alpha1 subunits (R528H). *FEBS Lett.* 423:198–204. https://doi.org/10.1016/S0014-5793(98)00090-8

Jurkat-Rott, K., M.A. Weber, M. Fauler, X.H. Guo, B.D. Holzherr, A. Paczulla, N. Nordsborg, W. Joechle, and F. Lehmann-Horn. 2009. K+-dependent paradoxical membrane depolarization and Na+ overload, major and reversible contributors to weakness by ion channel leaks. *Proc. Natl. Acad. Sci. USA.* 106:4036–4041. https://doi.org/10.1073/pnas.0811277106

Kim, A.M., and J.L. Vergara. 1998. Supercharging accelerates T-tubule membrane potential changes in voltage clamped frog skeletal muscle fibers. *Biophys. J.* 75:2098–2116. https://doi.org/10.1016/S0006-3495(98)77652-0

Lapie, P., C. Goudet, J. Nargeot, B. Fontaine, and P. Lory. 1996. Electrophysiological properties of the hypokalaemic periodic paralysis mutation (R528H) of the skeletal muscle alpha 1s subunit as expressed in mouse L cells. *FEBS Lett.* 382:244–248. https://doi.org/10.1016/0014-5793(96)00173-1

Liman, E.R., J. Tytgat, and P. Hess. 1992. Subunit stoichiometry of a mammalian K^+ channel determined by construction of multimeric cDNAs. *Neuron.* 9:861–871. https://doi.org/10.1016/0896-6273(92)90239-A

Matthews, E., R. Labrum, M.G. Sweeney, R. Sud, A. Haworth, P.F. Chinnery, G. Meola, S. Schorge, D.M. Kullmann, M.B. Davis, and M.G. Hanna. 2009. Voltage sensor charge loss accounts for most cases of hypokalemic periodic paralysis. *Neurology.* 72:1544–1547. https://doi.org/10.1212/01.wnl.0000342387.65477.46

Matthews, E., S. Portaro, Q. Ke, R. Sud, A. Haworth, M.B. Davis, R.C. Griggs, and M.G. Hanna. 2011. Acetazolamide efficacy in hypokalemic periodic paralysis and the predictive role of genotype. *Neurology.* 77:1960–1964. https://doi.org/10.1212/WNL.0b013e31823a0cb6

Mi, W., V. Rybalchenko, and S.C. Cannon. 2014. Disrupted coupling of gating charge displacement to Na^+ current activation for DIIS4 mutations in hypokalemic periodic paralysis. *J. Gen. Physiol.* 144:137–145. https://doi.org/10.1085/jgp.201411199

Miller, T.M., M.R. Dias da Silva, H.A. Miller, H. Kwiecinski, J.R. Mendell, R. Tawil, P. McManis, R.C. Griggs, C. Angelini, S. Servidei, et al. 2004. Correlating phenotype and genotype in the periodic paralyses. *Neurology.* 63:1647–1655. https://doi.org/10.1212/01.WNL.0000143383.91137.00

Moreau, A., P. Gosselin-Badaroudine, and M. Chahine. 2014. Biophysics, pathophysiology, and pharmacology of ion channel gating pores. *Front. Pharmacol.* 5:53. https://doi.org/10.3389/fphar.2014.00053

Morrill, J.A., and S.C. Cannon. 1999. Effects of mutations causing hypokalaemic periodic paralysis on the skeletal muscle L-type Ca2+ channel expressed in Xenopus laevis oocytes. *J. Physiol.* 520:321–336. https://doi.org/10.1111/j.1469-7793.1999.00321.x

Morrill, J.A., R.H. Brown Jr., and S.C. Cannon. 1998. Gating of the L-type Ca channel in human skeletal myotubes: an activation defect caused by the hypokalemic periodic paralysis mutation R528H. *J. Neurosci.* 18:10320–10334.

Nelson, B.R., F. Wu, Y. Liu, D.M. Anderson, J. McAnally, W. Lin, S.C. Cannon, R. Bassel-Duby, and E.N. Olson. 2013. Skeletal muscle-specific T-tubule protein STAC3 mediates voltage-induced Ca2+ release and contractility. *Proc. Natl. Acad. Sci. USA.* 110:11881–11886. https://doi.org/10.1073/pnas.1310571110

Polster, A., S. Perni, H. Bichraoui, and K.G. Beam. 2015. Stac adaptor proteins regulate trafficking and function of muscle and neuronal L-type Ca2+ channels. *Proc. Natl. Acad. Sci. USA.* 112:602–606. https://doi.org/10.1073/pnas.1423113112

Polster, A., B.R. Nelson, E.N. Olson, and K.G. Beam. 2016. Stac3 has a direct role in skeletal muscle-type excitation-contraction coupling that is disrupted by a myopathy-causing mutation. *Proc. Natl. Acad. Sci. USA.* 113:10986–10991. https://doi.org/10.1073/pnas.1612441113

Ruff, R.L. 1999. Insulin acts in hypokalemic periodic paralysis by reducing inward rectifier K+ current. *Neurology.* 53:1556–1563. https://doi.org/10.1212/WNL.53.7.1556

Schredelseker, J., M. Shrivastav, A. Dayal, and M. Grabner. 2010. Non-Ca2+-conducting Ca2+ channels in fish skeletal muscle excitation-contraction coupling. *Proc. Natl. Acad. Sci. USA.* 107:5658–5663. https://doi.org/10.1073/pnas.0912153107

Sokolov, S., T. Scheuer, and W.A. Catterall. 2005. Ion permeation through a voltage-sensitive gating pore in brain sodium channels having voltage sensor mutations. *Neuron.* 47:183–189. https://doi.org/10.1016/j.neuron.2005.06.012

Sokolov, S., T. Scheuer, and W.A. Catterall. 2007. Gating pore current in an inherited ion channelopathy. *Nature.* 446:76–78. https://doi.org/10.1038/nature05598

Sokolov, S., T. Scheuer, and W.A. Catterall. 2010. Ion permeation and block of the gating pore in the voltage sensor of $Na_V1.4$ channels with hypokalemic periodic paralysis mutations. *J. Gen. Physiol.* 136:225–236. https://doi.org/10.1085/jgp.201010414

Starace, D.M., and F. Bezanilla. 2001. Histidine Scanning Mutagenesis of Basic Residues of the S4 Segment of the *Shaker* K^+ channel. *J. Gen. Physiol.* 117:469–490. https://doi.org/10.1085/jgp.117.5.469

Starace, D.M., and F. Bezanilla. 2004. A proton pore in a potassium channel voltage sensor reveals a focused electric field. *Nature.* 427:548–553. https://doi.org/10.1038/nature02270

Sternberg, D., T. Maisonobe, K. Jurkat-Rott, S. Nicole, E. Launay, D. Chauveau, N. Tabti, F. Lehmann-Horn, B. Hainque, and B. Fontaine. 2001. Hypokalaemic periodic paralysis type 2 caused by mutations at codon 672 in the muscle sodium channel gene SCN4A. *Brain.* 124:1091–1099. https://doi.org/10.1093/brain/124.6.1091

Struyk, A.F., and S.C. Cannon. 2007. A Na^+ Channel Mutation Linked to Hypokalemic Periodic Paralysis Exposes a Proton-selective Gating Pore. *J. Gen. Physiol.* 130:11–20. https://doi.org/10.1085/jgp.200709755

Struyk, A.F., V.S. Markin, D. Francis, and S.C. Cannon. 2008. Gating Pore Currents in DIIS4 Mutations of $Na_V1.4$ Associated with Periodic Paralysis: Saturation of Ion Flux and Implications for Disease Pathogenesis. *J. Gen. Physiol.* 132:447–464. https://doi.org/10.1085/jgp.200809967

Tombola, F., M.M. Pathak, and E.Y. Isacoff. 2005. Voltage-sensing arginines in a potassium channel permeate and occlude cation-selective pores. *Neuron.* 45:379–388. https://doi.org/10.1016/j.neuron.2004.12.047

Wang, Q., M. Liu, C. Xu, Z. Tang, Y. Liao, R. Du, W. Li, X. Wu, X. Wang, P. Liu, et al. 2005. Novel CACNA1S mutation causes autosomal dominant hypokalemic periodic paralysis in a Chinese family. *J. Mol. Med. (Berl.).* 83:203–208. https://doi.org/10.1007/s00109-005-0638-4

Wu, F., W. Mi, D.K. Burns, Y. Fu, H.F. Gray, A.F. Struyk, and S.C. Cannon. 2011. A sodium channel knockin mutant (NaV1.4-R669H) mouse model of hypokalemic periodic paralysis. *J. Clin. Invest.* 121:4082–4094. https://doi.org/10.1172/JCI57398

Wu, F., W. Mi, E.O. Hernández-Ochoa, D.K. Burns, Y. Fu, H.F. Gray, A.F. Struyk, M.F. Schneider, and S.C. Cannon. 2012. A calcium channel mutant mouse model of hypokalemic periodic paralysis. *J. Clin. Invest.* 122:4580–4591. https://doi.org/10.1172/JCI66091